Best Practices for Accurate Results using Numerical Solvers for Microwave Body Screening

Raquel A. Martins[1], Daniela M. Godinho[2], João M. Felício[1,3], Matteo Savazzi[1,2], Jorge R. Costa[1,4], Raquel C. Conceição[2], Carlos A. Fernandes[1]

[1] Instituto de Telecomunicações, IST, Universidade de Lisboa, Lisboa, Portugal, raquel.martins@lx.it.pt

[2] Instituto de Biofísica e Engenharia Biomédica, Faculdade de Ciências, Universidade de Lisboa, 1749-016-Lisboa, Portugal

[3] Centro de Investigação Naval (CINAV), Escola Naval, Instituto Universitário Militar, Almada, Portugal

[4] ISCTE – Instituto Universitário de Lisboa (ISCTE-IUL), Lisboa, Portugal

***Abstract*—In this paper, we indicate best practices that should be observed when using numerical solvers for microwave body sensing. We show the impact of not minding these aspects in the case of microwave breast scanning, using the Computer Simulation Technology software tool. To this end we simulate a homogeneous breast with a 5-mm radius spherical tumor placed inside. The breast is illuminated by a broadband antenna that operates in the 2-6 GHz band. The scattering parameters are then processed to reconstruct the reflectivity map of the breast. The results highlight that the conclusions drawn from simulations may be misleading or meaningless when the solver type or positioning of model elements (body and antennas) are not carefully applied. This is particularly critical when considering more complex scenarios, such as inhomogeneous or multilayer body models.**

***Index Terms*—microwave breast imaging, electromagnetic numerical solvers, broadband simulation, time-domain simulation, frequency-domain simulation.**

I. INTRODUCTION

Over the last decades, Microwave Imaging (MWI) has been investigated as an alternative to conventional medical imaging modalities for different parts of the body [1]-[4]. The appeal of MWI lies in its non-ionizing and non-invasive nature, potential cost-effectiveness, and possibility to automate the imaging process.

In microwave (MW) imaging systems, the tissues are illuminated by one or several antennas, which transmit signals and retrieve the echoes originated by the contrast between the dielectric properties of benign and malignant tissues. Then, with the collected signals, a MW image can be created, and tumor detection can be investigated.

In a first approach, to evaluate a MW body screening system, researchers use numerical models to design/test a configuration. There is a variety of 3D electromagnetic simulators for developing numerical setups, however Computer Simulation Technology (CST) [5] and High-Frequency Structure Simulator (HFSS) [6] are among the most popular. Numerical software for high frequency simulations offers a variety of solvers, including time and frequency-domains. The first is generally preferred for broadband and electrically large simulations, whereas the second is mostly used for narrowband and electrically small models. Although this rule of thumb generally applies in MW device design (e.g. filters, antennas, etc.), there is no consensus in the MWI community, especially for biomedical applications. Researchers are generally well informed about the best settings that are required to obtain meaningful results from simulation, within reasonable computation time. However, there are specific aspects in the numerical modeling of biological tissues, antennas, etc., that may be not so well known.

To fill this gap, in this paper we present best practices that should be considered when using numerical solvers for MW body screening assessment. We show the impact that a non-attentive approach may have on target detection. To do so, we study the effects of considering inappropriate (i) solver domain and (ii) element (antennas and body) positioning.

This paper is organized as follows: in Sections II and III, we describe the numerical setup and the signal processing algorithms that we adopted to pursue our investigation; in Section IV, we discuss the frequency and time-domain solvers; in Section V, we study the influence of the positioning of the antenna and breast in the simulations; lastly, in Section VI we draw the conclusions.

II. NUMERICAL SETUP

To show the impact of misinformed approach to numerical assessment of microwave body sensing, we select the breast as the body part to analyze in our work. However, we emphasize that the conclusions can be extended to other body parts, since the challenges and limitations are inherently common. Moreover, although we use CST to design our simulation framework, the recommendations apply to other numerical simulation tools. This section describes the antenna and breast models used throughout the paper.

As depicted in Fig. 1, we assume a monostatic configuration, where the antenna scans the breast in the z=0 plane. The antenna consists of two crossed-exponentially tapered slots (XETS) [7] and is impedance-matched across the frequency range between 2 and 6 GHz, as proven in Fig. 2. The input reflection coefficient, $s_{11}(f)$, is logged every 30º degrees, in a total of 12 observations points, over a circle of 80-mm radius. The minimum, average and maximum

978-88-31299-09-1/24/$31.00 ©2024 IEEE

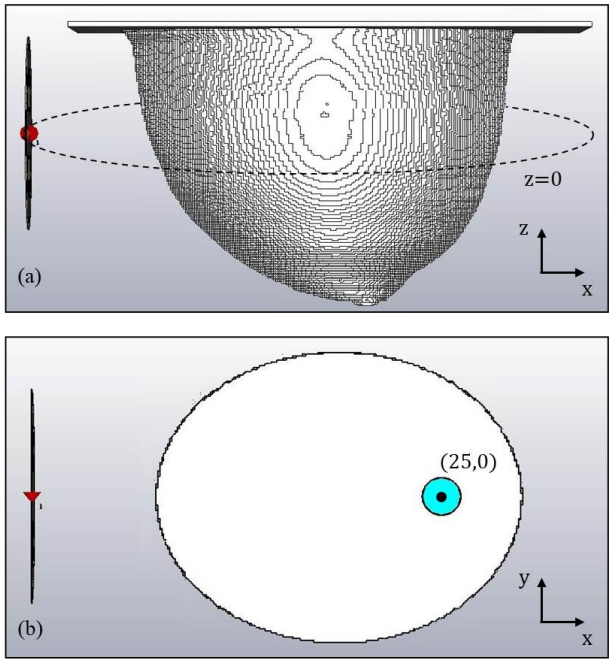

Fig. 1. Three-dimensional numerical breast setup from CST composed of an antenna, breast and a tumor: (a) xz-plane; (b) xy-plane.

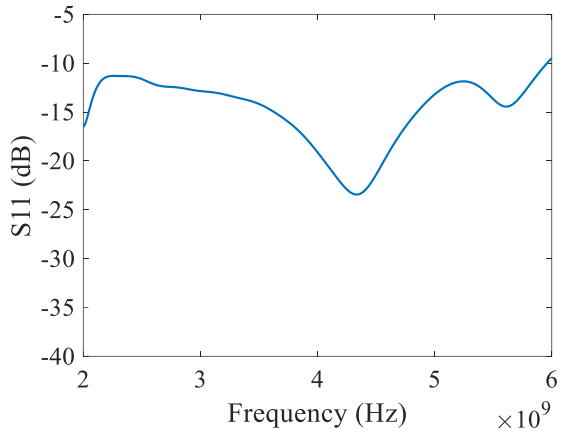

Fig. 2. Input reflection coefficient of the antenna in freespace, $s_{11}(f)$.

straight-line distance between the antenna and the breast is 32 mm, 37.8 mm, and 42.5 mm, respectively.

A three-dimensional breast shape is defined according to the ID 062204 model from the University of Wisconsin-Madison breast MRI-based repository [8]. Here, we consider a homogeneous breast, i.e., comprising only fat tissue. We did not contemplate skin layer in the model since its absence does not affect the results of this work. Also, we placed a 5 mm-radius spherical target mimicking a tumor inside the fat medium at position (25,0,0). The adipose tissue presents a dielectric constant of 8 and a loss tangent of 10^{-1}, whereas the tumor presents a dielectric constant of 60 and the same loss tangent, which are representative of real tissues [9]. Although the dielectric properties used are approximations of real ones, these do not interfere with the purpose of this study.

III. Signal Processing

Our analysis is based on the radar-based imaging results, obtained for each test case, or solver under test. This section describes the signal processing algorithms used to reconstruct the reflectivity map of the breast, namely the artifact removal and the wave-migration algorithms.

Prior to imaging the breast, it is necessary to remove the backscattering from the phantom surface. Here, we did so by calculating the difference between the reflection coefficients computed in the presence and in the absence of the tumor. Although it is not feasible in real practice, it allows presenting our point without possible masking by the artifact removal algorithm.

We considered an image reconstruction algorithm based on wave-migration. This algorithm back-propagates the phase of the wave radiated by the antenna and couples into the breast [10]. The contributions from all antenna positions, a, and frequency points, f, are summed for each pixel at coordinate (x, y), according to the following expression:

$$I(x,y) = \left| \sum_{a} \sum_{f} s_{11}^{cal}(f,a) e^{2jk_0(f)(d_b n_b + d_{air})} \right|^2 \qquad (1)$$

where $I(x,y)$ is the intensity of the pixel, $s_{11}^{cal}(f,a)$ is the reflection coefficient obtained after the calibration by the artifact removal, j is the imaginary unit, $k_0(f) = 2\pi f/c$ is the wavenumber in vacuum, d_b is the distance travelled by the wave inside the breast, d_{air} is the distance travelled in air (i.e. outside the breast), and n_b designates the refractive index of the breast tissues.

IV. Solver Domain

The use of an unsuitable solver may affect simulation performance. We tested both the time and frequency-domain solvers for the topic under study.

For both time-domain and frequency-domain generated data, Fig. 3 reports the resulting $s_{11}(f)$. Fig. 4 shows a comparison between breast imaging results using data generated with time-domain (Fig. 4 (a)) and frequency-domain (Fig. 4 (b)) solvers.

Ideally, if the simulation is configured with an appropriate number/size of mesh cells, results from both solvers should give very similar results. In both solvers, we adopted the default mesh number/size pre-defined by CST. While in time-domain, CST chooses a hexahedral mesh, in the frequency-domain, it chooses a tetrahedral mesh [11]. Hence, comparing the number of mesh cells is not meaningful.

Moreover, in the frequency-domain solver, there is a need to choose frequency points that cover the entire band to perform several simulations. For this case, we select 30 equidistant samples in the 2-6 GHz frequency range.

From Fig. 3, we can observe a slight difference between the behavior of the $s_{11}(f)$ curves for both domains. This tells

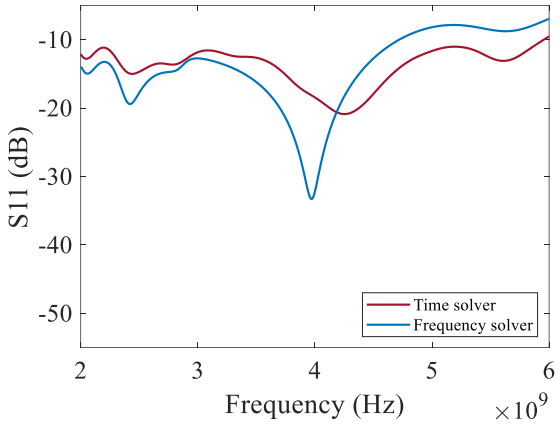

Fig. 3. $s_{11}(f)$ signals of the antenna response when using two different domain solvers (time and frequency).

TABLE I. SIMULATION TIMES FOR TIME AND FREQUENCY-DOMAIN

Numerical solver	*Simulation without tumor*	*Simulation with tumor*
Time	46 h, 42 min	47 h, 55 min
Frequency	56 h, 2 min	68 h, 18 min

that the number of mesh cells should have been increased. This would aggravate the computation time. TABLE I. shows the total evaluation time for simulations using the time and frequency-domain solvers with and without tumor using an Intel(R) Xeon(R) CPU E5649 @ 2.53 GHz with 64 GB RAM. Notice that no other process was running during these simulations.

Anyway, the results in Fig. 4 suggest that the choice of the solver (time or frequency-domain) does not affect the resulting images. However, it is worth reporting that, in the worst case, the frequency-domain simulation time was 21 hours higher than the time-domain simulation. This suggests the advantage of preferring a time-domain solver due to reduced computational costs when no imaging differences are observed.

Another important factor to mind is the choice of solver's convergence criterion. For the time-domain solver in CST, the default value is -40 dB, i.e., the solver stops when the remaining energy in the calculation decreases by -40 dB compared to the maximum energy. This is a critical factor, because the $s_{11}(f)$ associated with the tumor response may be lower than -60 dB. To assess the impact of decreasing this parameter in the application of breast cancer screening, Fig. 5 shows the $s_{11}(f)$ curves of the response of the tumor, obtained for solver accuracy of -40 and -80 dB for antennas closer (at 55 mm) and further away (at 105 mm) from the tumor. In this case, we considered a tumor with a 3-mm radius.

When using -80 dB accuracy, the simulation detects signal responses with lower magnitude than when -40 dB is used. For this case, both signals seem very similar within the working band of the antenna (2-6 GHz). Fig. 6 shows the imaging results obtained with the two solver accuracies: (a) -40 dB and (b) -80 dB. For this simple breast case, the tumor is detected with both settings. For clarity, Fig. 7 shows the reconstructed image difference between signals from simulations with -40 dB and -80 dB accuracy.

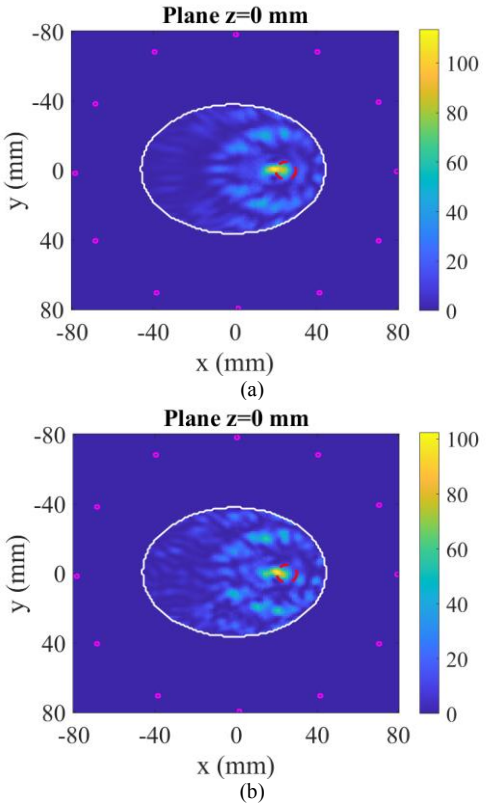

Fig. 4. Imaging results when using a (a) Time-domain simulation, and a (b) Frequency-domain simulation.

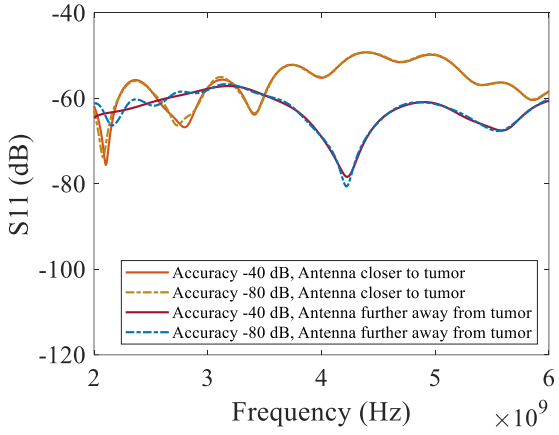

Fig. 5. $s_{11}(f)$ signals of only tumor response when setting solver accuracy to -40 and -80 dB. Two different angular positions (closer and further away from the tumour) are considered.

It is important to mention that in a more complex scenario, with a complete breast (considering fibroglandular tissue), where the tumor usually has a smaller intensity response, this parameter could have a much higher impact on tumor detection.

V. Rotation Considerations

In monostatic MWI, the most practical approach to simulating the movement of an antenna around an unknown object (e.g., a breast) in CST involves using the "Parameter Sweep" feature.

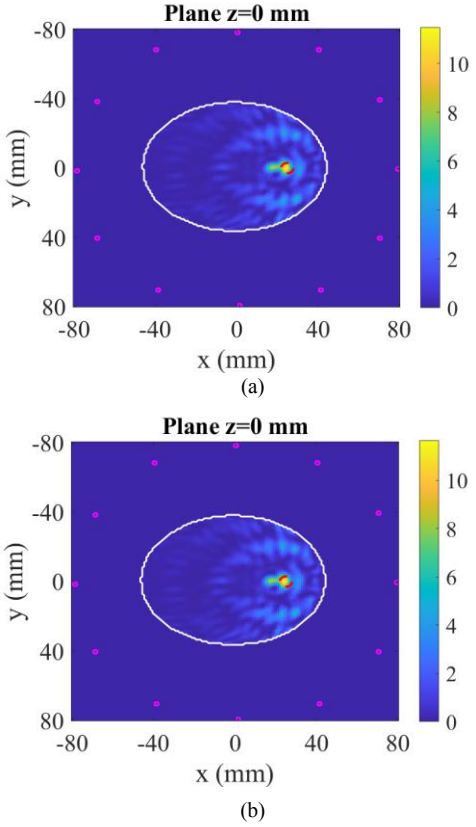

Fig. 6. Imaging results when using a Time-domain simulation with (a) −40 dB accuracy and (b) −80 dB accuracy.

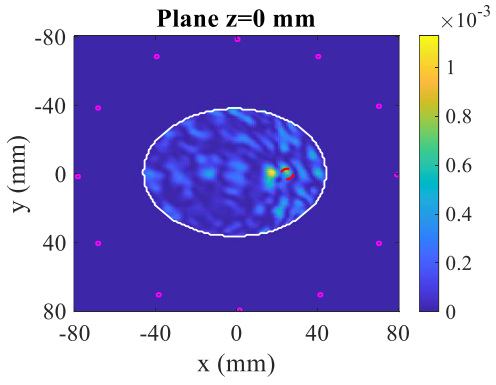

Fig. 7. Imaging results of the difference between signals from simulations with −40 dB and −80 dB accuracy.

This feature allows the association of a parameter with the rotation (or translation) of either the antenna or the breast. By using the "Parameter Sweep", a simulation will run for the specified values for that parameter, avoiding the increase of number of simulation files and their configuration. In this paper, we used "Parameter Sweep" to simulate a monostatic scan with 12 different angular positions of the antenna.

In order to simulate $s_{11}(f)$ acquisitions at different angular positions, one might consider rotating the antenna (and the source) around the breast, as shown in Fig. 8 (a) and (c). However, CST requires the source (discrete port or waveguide port) to always be aligned with the Cartesian planes defined in the CST model. Hence, rotating the antenna may affect the computation of the s-parameters when it compromises the alignment of the source with the Cartesian planes. For obtaining more reliable results, we recommend rotating the phantom (i.e., the breast), instead of the antenna, as shown in Fig. 8 (b) and (d).

To support our claim, we simulated four $s_{11}(f)$ acquisitions at two different relative angular positions between the antenna and the phantom, achieved by either rotating the antenna (+30º and +90º) or rotating the phantom (-30º and -90º) with respect to the reference position, as depicted in Fig. 8.

Fig. 9 illustrates the resulting $s_{11}(f)$ for the four cases. We observe that when the antenna is not orthogonal to the planes (i.e., after a +30º antenna rotation), the $s_{11}(f)$ differs from the $s_{11}(f)$ obtained with the same geometrical configuration after a -30º phantom rotation (source aligned to the Cartesian planes). Conversely, performing a +90º antenna rotation or a -90º phantom rotation produces consistent results, as the source is always aligned with the Cartesian planes.

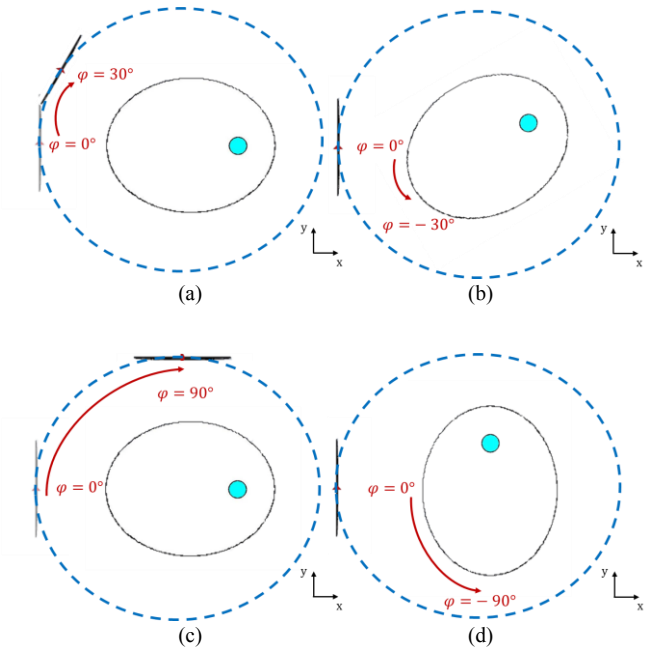

Fig. 8. Simulating an antenna position by fixing the breast and rotating the antenna (a) +30º or (c) +90º, or by fixing the antenna and rotating the breast (b) -30º or (d) -90º.

To understand the impact that rotation has on imaging results, the reconstructed image considering all 12 antenna positions is shown in Fig. 10. Although the target is still well-defined, as this is a simple scenario, the magnitude of the image decreases by 9.4%, if we consider the rotation of the antenna, instead of the opposite rotation of the phantom.

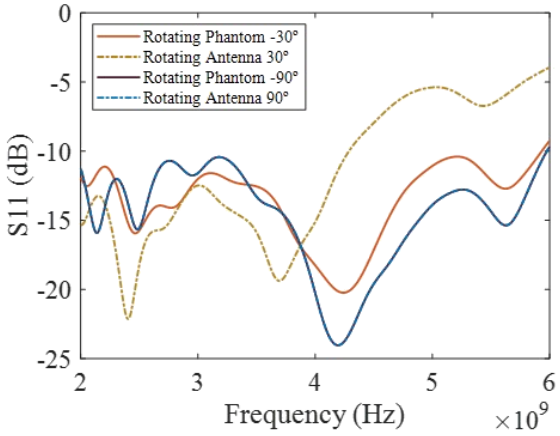

Fig. 9. $s_{11}(f)$ signals of the antenna response when rotating the antenna and rotating the phantom for two angular positions.

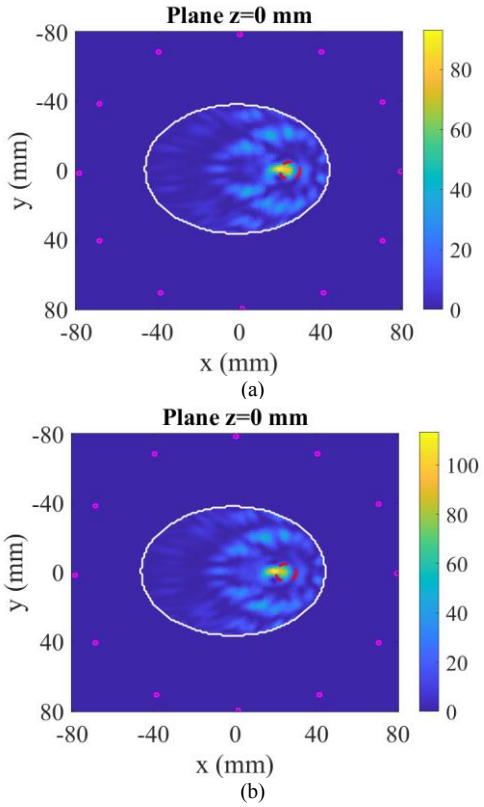

Fig. 10. Imaging results when (a) rotating the antenna, and (b) rotating the phantom.

VI. Conclusion and Future Work

This paper reviews some of the best practices that should be considered when using numerical solvers for MW body screening problems.

It focuses on the effects that a misinformed approach may have on target detection, when considering two main aspects: solver domain and positioning of elements. For demonstration, we used a simple representation of a breast and tumor to highlight those effects, and explain why some practices must be considered, especially in more complex body scenarios.

Although in this paper, we analyzed the effects produced in terms of signal response and imaging, it may impact other type of analysis not involving image reconstruction, like in the generation of datasets for machine learning training.

Acknowledgment

This work was funded by Fundação para a Ciência e Tecnologia (FCT/MCTES) through national funds under scholarship SFRH/BD/144961/2019, under the project 2022.08973.PTDC (https://doi.org/10.54499/2022.08973.PTDC), UIDB/00645/2020 (https://doi.org/10.54499/UIDB/00645/2020), and in part by FEDER under projects UIDB/50008/2020 and 2022.04764.PTDC (IRMIS).

References

[1] B. J. Mohammed, et al., "Microwave System for Head Imaging," IEEE Trans. Instrnm. Meas., vol. 63, no. 1, pp. 117-123, Jan. 2014.

[2] S. Kwon, and S. Lee," Recent Advances in Microwave Imaging for Breast Cancer Detection," Int. J. Biomed. Imaging, ID 5054912 pp. 1-26, 2016.

[3] A. Rezaeieh, et al. "Novel Microwave Torso Scanner for Thoracic Fluid Accumulation Diagnosis and Monitoring," Sci. Rep., vol. 7, no. 1, p. 304, 2017.

[4] D. M. Godinho, et al., "Experimental Evaluation of an Axillary Microwave Imaging System to Aid Breast Cancer Staging," IEEE J. Electromagn. RF Microw. Med., vol. 6, no. 1, pp. 68-76, March 2022.

[5] (September 2023). CST – Computer Simulation Technology [Online]. Available: https://www.cst.com/.

[6] (September 2023). Ansys HFSS | 3D Frequency Simulation Software [Online]. Available: https://www.ansys.com/products/electronics/ansys-hfss.

[7] J. M. Felício, et al., "Antenna Design and Near-field Characterization for Medical Microwave Imaging Applications," IEEE Trans. Antennas Propag., vol. 67, no. 7, pp. 4811 - 4824, July, 2019.

[8] M. J. Burfeindt, T. J. Colgan, R. O. Mays, J. D. Shea, N. Behdad, B. D. V. Veen, and S. C. Hagness, "MRI-derived 3-D-printed breast phantom for microwave breast imaging validation," IEEE Antennas Wireless Propag. Lett., vol. 11, pp. 1610-1613, 2012.

[9] M. Lazebnik, et al., "A Large-Scale Study of the Ultrawideband Microwave Dielectric Properties of Normal, Benign and Malignant Breast Tissues Obtained from Cancer Surgeries," Physics in Medicine and Biology, vol. 52, pp. 6093–6115, 2007.

[10] J. M. Felício, et al., "Microwave Breast Imaging using a Dry Setup," IEEE Trans. Comput. Imaging, vol. 6, no. 1, pp. 167-180, Jan., 2020.

[11] T. Weiland, M. Timm and I. Munteanu, "A practical guide to 3-D simulation," in IEEE Microwave Magazine, vol. 9, no. 6, pp. 62-75, December 2008, doi: 10.1109/MMM.2008.929772.